Asian Journal of Water, Environment and Pollution, Vol. 21, No. 3 (2024), pp. 77-85.
DOI 10.3233/AJW240037

Experimental Study on the Removal of Toluene from Water by PTFE Hydrophobic Microporous Membrane Using Air Gap Membrane Distillation Process

Divya Gaur, Kailash Singh and Sushant Upadhyaya*
Department of Chemical Engineering, Malaviya National Institute of Technology, Jaipur – 302017, India
✉ supadhyay.chem@mnit.ac.in

Received May 12, 2024; revised and accepted May 18, 2024

Abstract: Toluene is used for various purposes such as a cleansing agent, paint thinner, lacquers, printing, and leather tanning process. However, it has an adverse effect on human bodies, such as skin irritation, leukemia, respiratory issues, mutagenicity, etc, when the chemical gets mixed in drinking and rainwater by the above routes. Therefore, there is a threat to the environment and society because of the presence of toluene in water bodies through industrial effluent. Henceforth, in this study, toluene is separated from water using the air gap membrane distillation (AGMD) process. The hydrophobic microporous poly-tetra- fluoro-ethylene has been employed for this purpose. Primarily, this work focussed on the study of operating parameters such as feed solution temperature and coolant temperature on the AGMD performance namely permeate flux and toluene selectivity. It was observed that the permeate flux increased exponentially from 2.07 kg/m^{2}h to 9.23 kg/m^{2}h, and 0.94 kg/m^{2}h to 3.53 kg/m^{2}h. However, it was found that the permeate flux decreased from 9.48 kg/m^{2}h to 8.12 kg/m^{2}h, and 3.78 kg/m^{2}h to 2.42 kg/m^{2}h on increasing the coolant temperature from 5°C to 25°C at 3 mm and 11 mm air gap, respectively. The membrane selectivity was found to be less than 1, which signifies the efficient toluene-water separation. In order to study the membrane performance in the long run, the permeate flux was estimated continuously till 60 h wherein the estimated flux was found to be almost constant. The membrane morphology before and after the 60 h experimental run was analysed using capture FE-SEM micrographs. The toluene concentration was estimated using a spectrophotometer at a wavelength of 264 nm.

Key words: toluene, hydrophobic PTFE membrane, SEM, selectivity, UV-Vis spectrophotometer.

Introduction

Abundant water is available on the earth's surface, however, due to rapid industrialisation, it has been observed that the quality of water is deteriorating as a result creating a threat to the environment. As per the United States Geological Survey (USGS), the oceans contain approximately 97% of the earth's water supply, of which 3% is fresh-water. Consequently, human-usable water comprises a mere 1% of the total water available on the planet (van Vliet et al., 2021). Water, being an essential resource for life, is presently in limited supply, impacting approximately one-fifth of the global population. Furthermore, a quarter of the world's population faces technological challenges in extracting freshwater from ponds and rivers. This critical issue of water scarcity is a direct consequence of population growth and industrial and agricultural development. According to the World Water Development Report 2015 of the United Nations, there is an estimated 40% scarcity of potable water worldwide by 2030, a span of merely fourteen years. The anticipated water

*Corresponding Author

scarcity and shortage can be mitigated through the implementation of sustainable water practices, effective wastewater treatment methods, and the acquisition of freshwater sources. The sole viable approach to augmenting the current freshwater reserves is through the purification of the salty ocean waters, which make up 97% of the earth's total water volume. Water scarcity is projected to place India at the 40th rank globally by the year 2040 (Manju and Sagar, 2017). In the industrial sector, toluene is extensively employed as a solvent for equipment cleansing, organic synthesis, and various subsequent processing objectives. Leaks in underground storage containers and pipelines, improper waste disposal practices, unintentional spills, and leaching from landfills are common sources of their presence in groundwater. These contaminants induce a variety of severe adverse health effects in humans, including irritation of the skin, central nervous system problems, respiratory issues, leukemia, cancer, and issues related to kidney, liver, and blood systems (Gaur et al., 2022). Due to the flammability, toxicity, carcinogenicity, and mutagenicity of toluene and its derivatives, it creates significant environmental hazards even present in trace amounts in the aqueous solution (Pui et al., 2019). Therefore, it is imperative to eliminate these organic pollutants from the water and effluent in order to safeguard water supplies. For toluene removal, membrane distillation (MD) has gained interest because of its compactness, operability at low temperatures and pressures, and less fouling are some of the benefits that distinguish this technique from conventional membrane processes like reverse osmosis (Pedram et al., 2019). MD process can be employed with the integration of other processes such as solar energy, and geothermal heat resources which makes the process energy efficient (Pangarkar et al., 2016). The MD process has several advantages, including chemical purification and concentration, food processing, heavy metal removal, acid saline effluent, ammonia, and volatile organic compounds removal from wastewater (Zare and Kargari, 2018). There are four distinct configurations of the MD process that can be categorised according to the condensation method: (a) DCMD, which involves a condensing fluid in direct contact with the membrane, (b) VMD, where vacuum is applied at the permeate side for desalination and dye removal (Baghel et al., 2020; Upadhyaya et al., 2016), (c) SGMD, where sweeping gas is circulated continuously at the permeate side, and (d) AGMD where stagnant gases namely helium, argon, and air are maintained in the permeate channel. The latter configuration is primarily used for azeotropic separation (Kalla et al., 2019b) and organic volatile components removal (Elhenawy et al., 2020; Kalla et al., 2019a). AGMD is the most advantageous configuration among all others in which stationary air is positioned between the membrane and condensation surface. At the interface between the liquid and the membrane, the liquid evaporates, and the evaporated component traverses the membrane. After passing through the air gap, the liquid condenses on the refrigerant plate in the air gap section. At the interface of the heated feed and membrane, water and the volatile component evaporate due to the temperature difference between the aqueous feed mixture and the cold surface. Similar to other membrane distillation configurations, AGMD operates on the principle of vapour-liquid equilibrium where mass and thermal transfer occur concurrently across the membrane. The air gap in this particular configuration confers an advantage by mitigating the problem of heat loss (Cai et al., 2020; Leaper et al., 2019).

It has been observed that toluene is removed primarily by adsorption by several authors (Stähelin et al., 2018; Zhao et al., 2018), however, its separation from aqueous solution is not found in the literature by the AGMD process. In viewpoint, AGMD may have great potential in the separation of organic solvents due to the selective transport of components based on its diffusivity in stagnant gases namely air, helium, and argon. Therefore, in this study, the separation of toluene from water is one of the main objectives. Moreover, few authors have studied the impact of various operating parameters on permeate flux for benzene removal by AGMD; however, the impact of operating parameters such as feed solution temperature on the second performance parameter i.e., selectivity is not observed in the literature. From per viewpoint, the system selectivity estimation will be the deciding factor in understanding the effectiveness of the AGMD process towards the level of separation. Therefore, in this work, the impact of operating variables, namely, feed solution temperature and coolant temperature on toluene selectivity as well as permeate flux were considered to determine the performance of the process. It is noteworthy to highlight that AGMD process performance for volatile organic binary system separation under continual long-run operation was overlooked by the researchers. Henceforth, AGMD process performance with respect to time was also considered to understand any efficacy of fouling phenomena on the membrane performance. The fouling study in this work was examined using FE-SEM morphology.

Material Required

The poly-tetra-fluoro-ethylene (PTFE) hydrophobic membrane of nominal pore sizes 0.22 µm was procured from Millipore manufacturer. The properties of the PTFE membrane are represented in Table 1. The deionised-water was made from tap water in the lab using traditional distillation equipment. A.C.S. grade toluene (>99.0%, EMPLURA) reagent was purchased from Abhishek Chemicals Co., Ltd., Jaipur for making a stock solution of toluene-water system.

Table 1: Physical properties of membrane

Properties	*Range*
Module Diameter (mm)	90
Hydraulic Diameter (mm)	45
Material	PTFE
Porosity (%)	85
Thickness (µm)	150
Pore Size (µm)	0.22
Manufacturer	Millipore

AGMD Setup and Experimental Procedure

In this investigation, an in-house fabricated AGMD experimental setup was used to separate the aqueous solution of the toluene-water system. The schematic representation of the fabricated AGMD setup is depicted in Figure 1. The membrane module of the AGMD set up is structured into four distinct segments namely feed portion, membrane segment, air gap channel and coolant section. In this study, the feed solution of the toluene-water system was heated to the required temperature using a heating apparatus situated at the base of the feed tank. The heated feed solution of 1000 mg/L toluene concentration was then pumped from the feed tank to the feed channel of the membrane module. The excess flow was bypassed in order to maintain the feed flow rate constant. The feed flow rate was maintained using rotameters (Starflow make) which were installed between the membrane module and feed tank. The vapour at the feed side penetrates the hydrophobic microporous membrane and condenses on the cooling plate in the air gap section. The resultant permeate product was then collected in the glass receiver. The retentate stream was continuously rejected and separated from the feed section. The temperature of the feed solution was controlled using a temperature controller which is connected to the heater. The coolant water was circulated continuously from the chiller towards the cooling channel in order to maintain the temperature of the cooling channel constant. The Type-J thermocouples measure the temperature at numerous junctions such as feed tank, feed side membrane surface, air gap side, and cooling channel. The specifications of the instruments connected in the AGMD set up are enumerated in Table 2. The permeate concentration was measured using a spectrophotometer (UV-1900, Labman) at 264 nm wavelength.

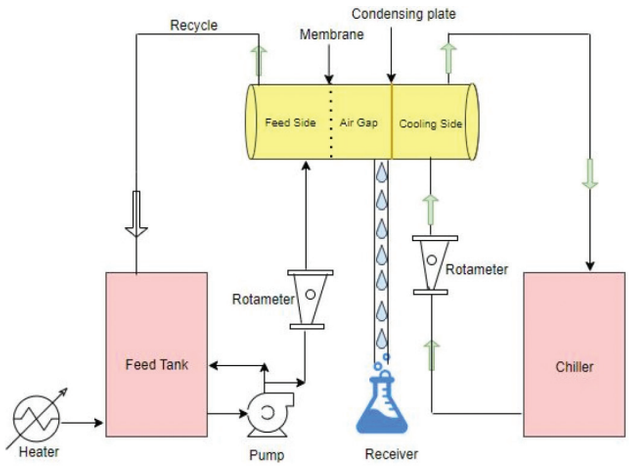

Figure 1: Schematic representation of AGMD configuration.

Table 2: Detailed description of instruments in AGMD configuration

Instrument	*Specification*	*Manufacturer*
Feed Pump	Capacity: 10 L/min Head: 3-4 meter Motor: 0.5 HP, 2900 RPM. 220 v	Leakless Pumps & Sealings Equipments. Mumbai, India
Cooling Pump	Capacity: 10 L/min Head: 3-4 meter Motor: 0.5 HP	Prasad Overseas. Jaipur, India
Chiller	Capacity: 50 L, Operating temperature: -15 to 25°C	M/s LABROS INSTRUMENTS. Jaipur
Rotameter	Range: 1-10 L/min	Starflow. India
Thermocouple	Type J Digital Thermocouples. PT-100	Techno Instruments. Gujarat

Analysis of the AGMD Process Separation Performance

The separation performance is assessed with respect to two key factors: selectivity and flux.

In this work, the performance of the AGMD process is determined by experimentally calculating the permeate flux and concentration of the toluene in the

permeate stream. The experimental flux is determined using equation 1, outlined as:

$$N_{flux} = \frac{V_P \times \rho_P}{A_m \times t} \quad (1)$$

where N_{flux}, V_p, ρ_p, A_m and t are total permeate flux (kg/m^{2}h), the volume of permeate collected (m^3), permeate density (kg/m^3), area of membrane (m^2), and a collection time (h).

The second performance parameter as toluene concentration in the permeate section is converted into selectivity (separation factor) and estimated using equation 2 as follows:

$$\alpha = \left(\frac{y/(1-y)}{x/(1-x)} \right) \quad (2)$$

where, α, y and x are the toluene selectivity, toluene mole fraction in permeate, and toluene mole fraction in retentate, respectively.

Results and Discussion

In this study, various sets of experiments were conducted to understand the impact of feed solution temperature ranges from (40°C-60°C) on permeate flux and selectivity of the AGMD process at constant feed flow rate of 3l/min under air gap ranges from 3 mm to 11 mm. Similarly, the effect of coolant temperature ranges from 5°C to 25°C was also studied at a constant feed solution temperature of 60°C for varying ranges of air gaps. The feed concentration of toluene and coolant flow rate were maintained at 1000 mg/L and 4 L/min, respectively.

Feed Temperature

The impact of feed solution temperature on total flux can be depicted in Figure 2. It was observed that at feed toluene concentration of 1000 mg/l, the total flux increases exponentially from 2.07 kg/m^{2}h to 9.23 kg/m^{2}h, 1.26 kg/m^{2}h to 5.04 kg/m^{2}h, and 0.94 kg/m^{2}h to 3.53 kg/m^{2}h on enhancing the feed solution temperature from 40°C- 60°C at air gap 3mm, 7mm, and 11mm respectively under feed flow rate of 3l/min, coolant temperature of 10°C. This may be attributed to the fact that vapour pressure of toluene and water increases exponentially with temperature as per the Antoine Equation (Kalla et al., 2019b). This relationship can be illustrated in Figure 3. Alternatively, the reason can be attributed to the fact that at elevated temperatures of the feed solution, the fluid viscosity (v) decreases,

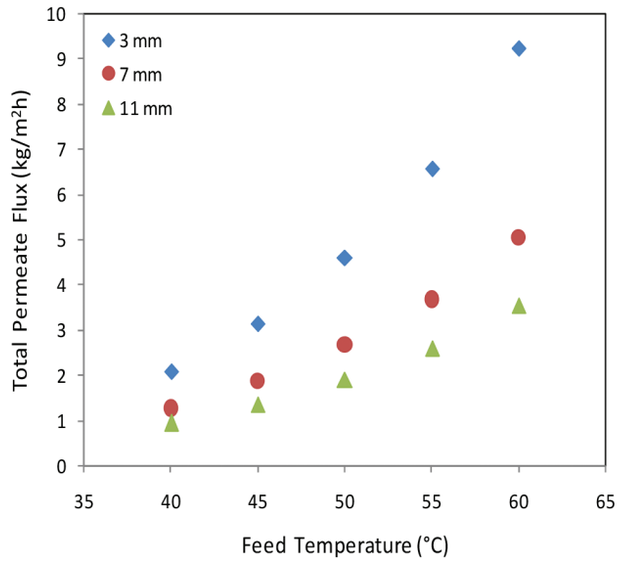

Figure 2: Impact of feed solution temperature on total permeate flux.

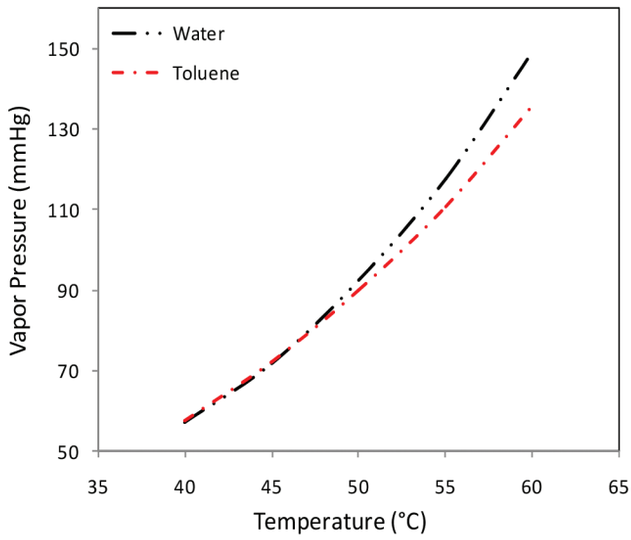

Figure 3: Temperature versus Vapour pressure plot.

resulting in the increase of the heat transfer coefficient of fluid $h_f \propto \frac{1}{v^{0.5}}$ (Baghel et al., 2020) which in turn increased the permeate flux tremendously. From Figure 2, it was also observed that an increase in permeate flux was also noted at an air gap of 3 mm relative to 11 mm. This reason may be because the mass transfer resistance for the lower air gap is less as compared to the higher air gap.

From Figure 4, it was depicted that individual flux increased from 2.03 kg/m^{2}h to 8.00 kg/m^{2}h and

0.04 kg/m^{2}h to 1.23 kg/m^{2}h for water and toluene respectively at a 3 mm air gap. The permeate flux of water is found to be higher than toluene. This reason is understood by calculating the diffusivities of water and toluene in the air by combining the kinetic theory of gases and corresponding states in terms of the temperature-dependent diffusivities (Bird, 2002) of individual components as shown in equation 3. The water diffusivity in the air is estimated and found to be increased from 2.90×10^{-5}m^2/s to 3.35×10^{-5}m^2/s whereas toluene diffusivity in the air increased from 1.27×10^{-5}m^2/s to 1.46×10^{-5}m^2/s on elevating the solution temperature from 40°C to 60°C. From the calculation, it is evident that the water diffusivity at any given temperature is approximately two times greater than that of toluene in air. As a result, water vapour will diffuse in huge amounts through the microporous membrane into the air gap as compared to toluene.

$$\frac{pD_{ia}}{\left(p_{Ci}p_{Ca}\right)^{1/3}\left(T_{Ci}T_{Ca}\right)^{5/12}\left(\frac{1}{M_i}+\frac{1}{M_a}\right)^{1/2}} = a\left(\frac{T}{\sqrt{T_{Ci}T_{Ca}}}\right)^{b} \tag{3}$$

where, $D_{ia}, p_{Ci,}$, $T_{Ci,,}$ and M_i are the diffusivity, critical pressure, critical temperature and molecular weight of component i in the air whereas $p_{Ca,}$, $T_{Ca,}$ and M_a are critical pressure, critical temperature, and molecular weight of air. The dimensionless constants a and b are taken from 3.64×10^{-4} and 2.334 respectively from the literature (Bird, 2002).

The preferential transfer of toluene in permeate is analysed by determining the concentration of toluene in permeate using a *UV* Spectrophotometer and thereafter the selectivity using equation 2 with respect to feed temperature. From Figure 5, it was found that toluene selectivity is less than 1 under the range of 40°C to 60°C which clearly endorses the selective transfer of water vapour in the permeate section. It is also observed that the selectivity decreased from 0.71 to 0.68, and 0.69 to 0.67 at 3 mm and 5 mm respectively on elevating the solution temperature from 40°C to 60°C. This proclaims that the weight fraction of toluene in permeate reduced by increasing the feed temperature. The decreasing trend in toluene selectivity and decrement in toluene concentration in permeate with increased feed temperature can be understood by the following thermodynamic expression equation 4 (Brouwer et al., 2021) of selectivity for the non-ideal solution under vapour- liquid equilibrium:

$$\alpha_{i,j} = \frac{\frac{y_i}{x_i}}{\frac{y_j}{x_j}} = \frac{\left(\frac{\varphi_i^L}{\varphi_i^v}\gamma_i\psi_i\frac{p_i^o}{P}\right)}{\left(\frac{\varphi_j^L}{\varphi_j^v}\gamma_j\psi_j\frac{p_j^o}{P}\right)} = \left(\frac{\varphi_i^L\varphi_j^v}{\varphi_i^v\varphi_j^L}\right)\left(\frac{\gamma_i}{\gamma_j}\right)\left(\frac{p_i^o}{p_j^o}\right) \tag{4}$$

where, subscript i and j stand for more and less volatile component, respectively.

x and y are the mole fractions of the component in the liquid and vapour phase, ϕ^L and ϕ^v are the fugacity coefficients of the component in the liquid and vapour phase, γ is the fugacity of the pure component, ψ is the

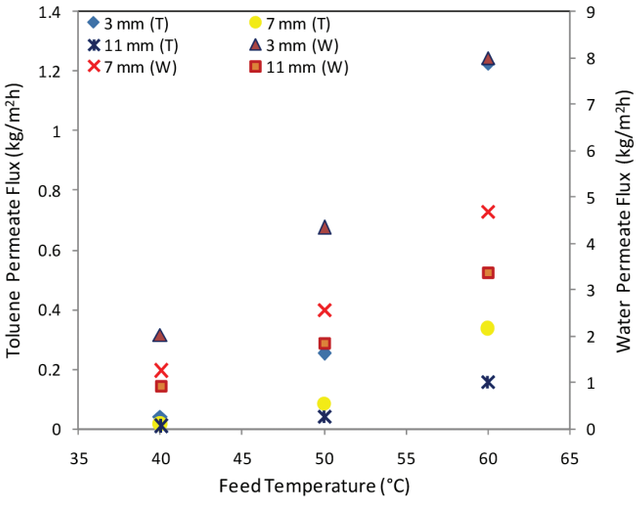

Figure 4: Impact of feed solution temperature on individual permeate flux.

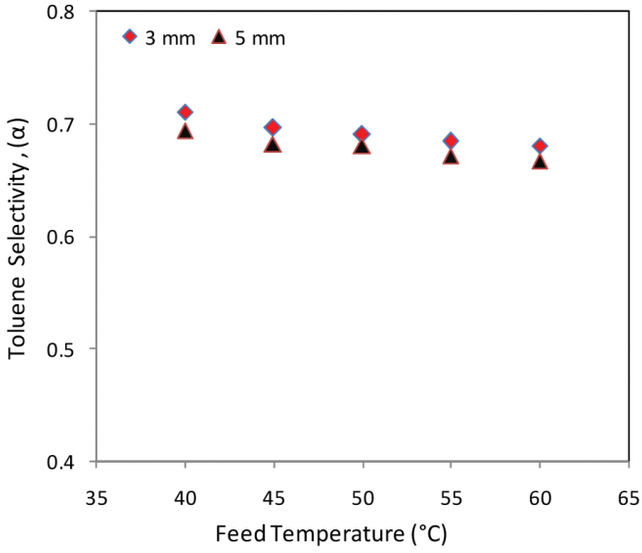

Figure 5: Impact of feed solution temperature on selectivity.

Poynting factor, $p°$ is vapour pressure of the component and P is the system pressure.

The Cox chart reveals that on increasing the temperature, the vapour pressure of the less volatile component increased at a faster rate as compared to the more volatile component. It is evident from equation 4, that the selectivity (separation factor) is directly proportional to the ratio of vapour pressure of more volatile to less volatile for non-ideal solution, as a result, selectivity decreases and separation may become tedious at a higher temperature when α approach to 1. Therefore, it can be corroborated that selectivity is inversely proportional to the temperature.

Coolant Temperature

Figure 6 illustrates the impact of coolant temperature on total flux under innumerable air gaps. It was observed that permeate flux decreased from 9.48 kg/m^{2}h to 8.12 kg/m^{2}h, 5.76 kg/m^{2}h to 3.92 kg/m^{2}h, and 3.78 kg/m^{2}h to 2.42 kg/m^{2}h on increasing the coolant temperature from 5°C to 25°C an air gap of 3mm, 7mm, and 11mm under feed toluene concentration of 1000 mg/l, feed flow rate of 3l/min, feed solution temperature of 60°C, and coolant flow rate of 4l/min. The total permeate flux declines due to the reduction in the thermal driving force between the feed solution temperature and cooling channel temperature (Elhenawy et al., 2020). In deeper scientific understanding, on increasing the coolant temperature, the coolant side heat transfer coefficient (h_c) decreases as a result the overall heat transfer coefficient (U) decreased as per the following equation 5 (Banat et al., 1999):

$$U = \frac{1}{\left(\frac{1}{h_f}\right)+\left(\frac{1}{h^*}\right)+\left(\frac{1}{h_c}\right)} \tag{5}$$

where, h_f, h^* *and* h_c are the heat transfer coefficient at the feed side (W/m^{2}K), air gap side (W/m^{2}K) and coolant side in (W/m^{2}K) respectively whereas U is the overall heat transfer coefficient.

The coolant side heat transfer coefficient is described by equation 6 as follows (Banat et al., 1999):

$$h_c = 0.943\left[\frac{\rho_1^{\,2} g\lambda k_l^{\,3}}{L\mu_1\Delta T_c}\right]^{1/4} \tag{6}$$

where, ρ_1, g λ, k_l, L, μ_1 and ΔT_c are the coolant fluid density, acceleration due to the gravity, enthalpy of vaporization, thermal conductivity, the height of air gap, viscosity and cooling temperature difference between inlet and outlet stream respectively.

The effect on individual permeate flux by coolant temperature is represented in Figure 7. The same declining trend in individual flux with coolant temperature was observed under various air gaps. Moreover, the water permeate flux was determined to be 8.22 kg/m^{2}h and 7.04 kg/m^{2}h at 5°C and 25°C coolant temperatures which was far higher than the toluene permeate flux of 1.25 and 1.05 kg/m^{2}h under same operating conditions. Though the thermal driving force between the boiling point of toluene and coolant temperature is higher than the thermal driving force between water and cooling temperature, the permeate

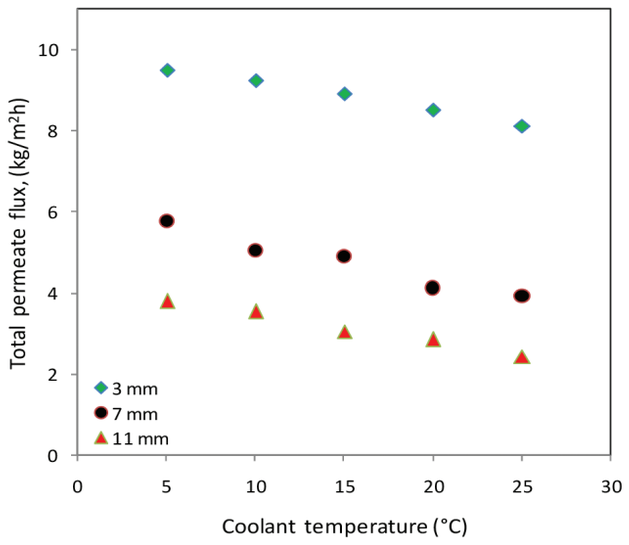

Figure 6: Impact of coolant temperature on permeate flux.

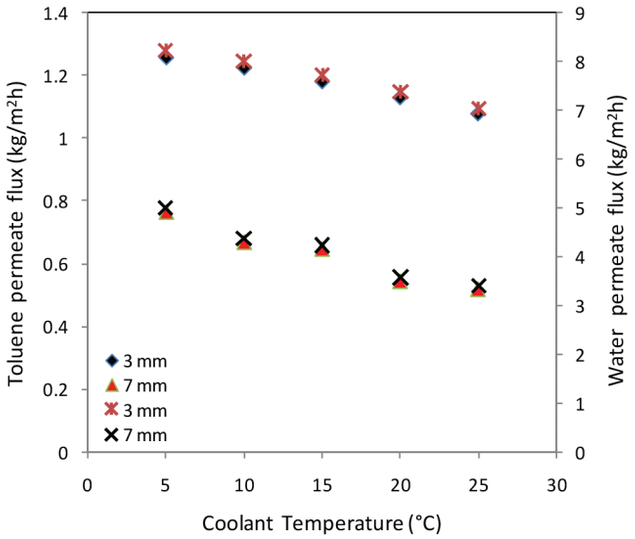

Figure 7: Impact of coolant temperature on individual flux.

flux of water is greater than toluene due to the reason that mass diffusivity of water in air is approximately 2.26 times higher than mass diffusivity of toluene in air which in turns enhance the film mass transfer coefficient (k) of water as compared to toluene since mass transfer coefficient is directly proportional to $D_{i-a}^{0.5}$ as per Danckwert's surface renewal theory (Khan, 1990). Therefore, the diffusive mass transfer rate for water is higher than that of toluene which proclaims an interesting result that mass transfer predominates the thermal driving force. The effect on toluene selectivity with respect to coolant temperature is depicted in Figure 8. It is indisputable that separation of toluene takes place as selectivity is less than 1 under various air gaps. Moreover, it was observed that the toluene selectivity is unvaryingly constant with cooling temperature. This clearly indicates the AGMD process is relevant for toluene-water separation.

Fouling Study

The membrane performance for the longer run was determined by studying the fouling phenomena on the surface of the PTFE membrane. The feed solution of toluene concentration 1000 mg/L was continuously fed with a feed flow rate of 3 L/min to the membrane module of the AGMD setup. The permeate flux was continuously collected from the air gap section till 60 h. The feed solution temperature, coolant flow rate, and coolant temperature were kept constant at 60°C, 4L/min. and 10°C, respectively. Based on Figure 9, it was observed that permeate flux was 9.23 kg/m^{2}h which was approximately constant till a continuous run of 60 h. This is clearly evident that the fouling phenomenon is insignificant with time and shows the potential removal of toluene from the toluene-water system. This could potentially be attributed to the absence of nonvolatile solutes in the feed otherwise they may adhere on the membrane surface by virtue the surface porosity and pore diameter get reduced and ultimately alter the permeate flux.

The fouling study was also extended by examining the captured FE-SEM membrane morphology of the new brand and used PTFE membrane after 60 h of continuous run as shown in Figures 10 and 11 respectively. From these FE-SEM micrographs, it was also endorsed that there was no significant fouling on the membrane surface because the surfaces of both images are almost identical due to the volatile nature of the feed component thereby permeate flux remains constant on a continual run of AGMD set up. The fouling phenomena on the membrane surfaced is primarily due to non-volatile inorganic salts however, in the present study, both the migrating components across the membrane surface are volatile therefore, the accumulation of these components on the pore of the membrane surface will not take place and finally the permeate is collected from the air gap section unvaryingly in continual hours of run. Furthermore, the membrane equivalent pore diameter was estimated using equation 7 (Phattaranawik et al., 2003) and the pore size distribution used and fresh membranes was plotted using *Image J* software as depicted in Figure

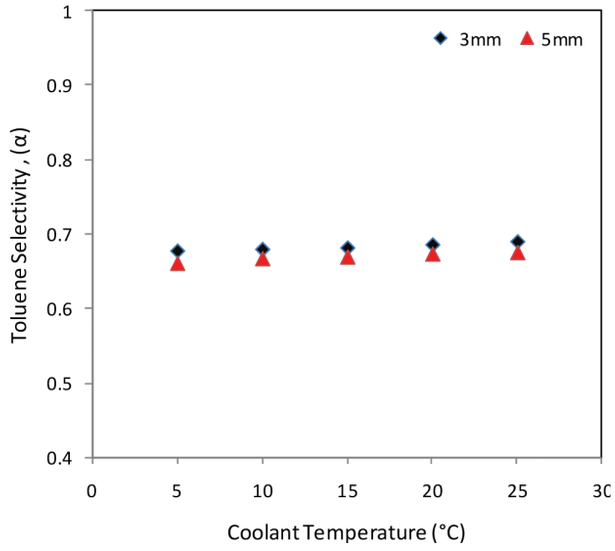

Figure 8: Impact of coolant temperature on toluene selectivity.

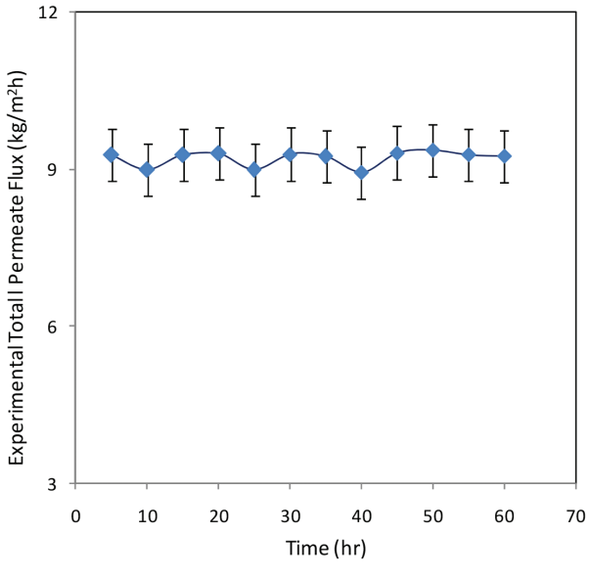

Figure 9: Effect of permeate flux on time.

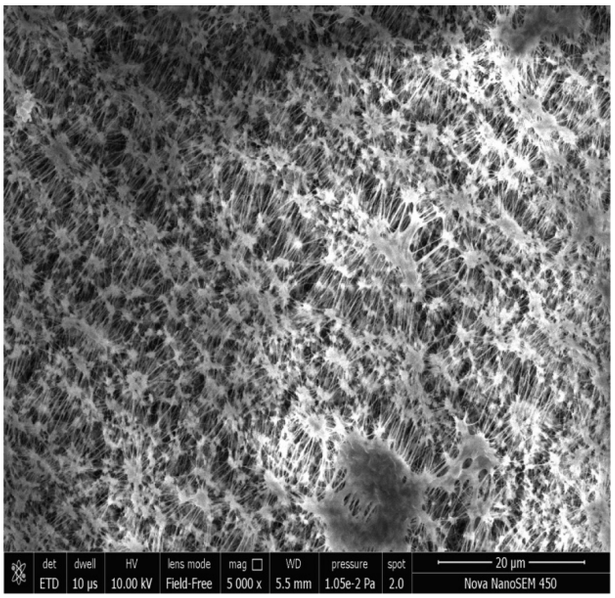

Figure 10: FE-SEM of the fresh membrane at 5,000 × magnification.

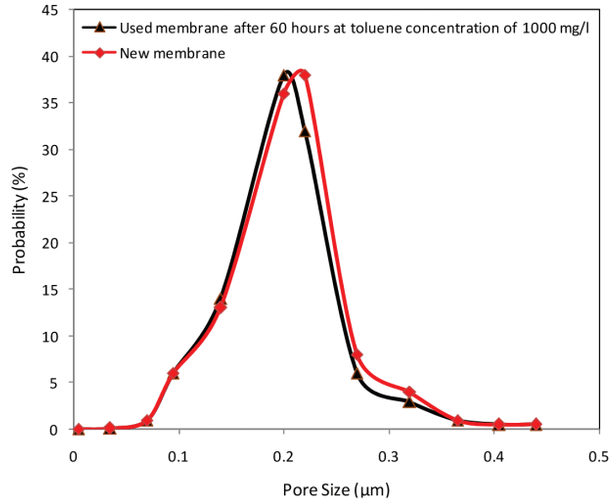

Figure 12: Pore size distributions for new membrane and used membrane.

12. The average pore size of the new brand membrane was estimated to be 0.22µ which was also claimed by the manufacturer (Millipore). Moreover, there was no reduction in the average pore size of the used and new membrane. This clearly proclaimed that the membrane allows the volatile component to penetrate in the air gap section without compromising its surface properties. As a result the membrane performance in terms of permeate flux remains intact with time.

$$d_{eq} = 2\sqrt{A_m / \pi} \tag{7}$$

where d_{eq} is the equivalent pore diameter of the membrane.

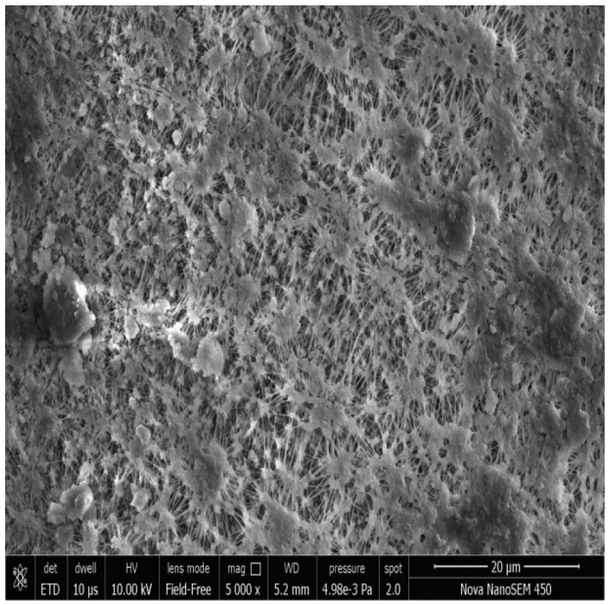

Figure 11: FE-SEM of used membrane at 5,000 × magnification.

Conclusion

In this study, a hydrophobic microporous PTFE membrane was utilised to separate the toluene-water system using the AGMD system. The influence of the most dominating operating parameters namely feed solution temperature and coolant temperature on separation performance i.e., total permeate flux, individual component flux, and toluene selectivity based on permeate collected was investigated thoroughly. It was observed that total permeate flux as well as toluene and water flux increased exponentially on increasing the feed solution temperature under various ranges of air gaps. At 60°C, the permeate flux was found to be a maximum of 9.23 kg/m^{2}h. The second performance parameter toluene selectivity was found to be less than 1 under the range 40°C to 60°C for feed solution temperature which shows the efficient separation of toluene-water system. Moreover, it further decreased on increasing the temperature and proclaims that AGMD has potential in the separation of an organic mixture. It was observed that the permeate flux exhibited a linear increase as the coolant temperature decreased, whereas the toluene selectivity was almost constant and found to be 0.69 and 0.67 for 3 mm and 5 mm respectively. The membrane performance under long run was also examined and it was observed that permeate flux was constant throughout till 60 h continuous run which clearly indicates the absence of fouling phenomena. No remarkable variation in the membrane morphology

was seen on the captured FE-SEM micrographs (5000× magnifications) of the new and used membrane. Furthermore, from the pore size distribution (PSD) plot developed using *Image J* software, the average pore diameter of the used membrane was detected at 0.21 micron which was approximately the same as that of the new membrane pore size (φ=0.22 micron). These micrographs and PSD clearly endorsed that permeate flux was constant under the continual operation of 60 h. Finally, it can be concluded that AGMD has great potential in the separation of toluene-water and other organic systems which reduces the burden on the environment towards sustainable separation.

References

Baghel, R., Kalla, S., S.,Chaurasia, S. and K. Singh (2020). CFD modeling of vacuum membrane distillation for removal of naphthol blue black dye from aqueous solution using COMSOL multiphysics. *Chemical Engineering Research and Design*, **158**: 77-88.

Banat, Fawzi A. and J. Simandl (1999). Membrane distillation for dilute ethanol: separation from aqueous streams. *Journal of Membrane Science*, **163(2):** 333-348.

Bird, R.B., Stewart, W.E. and E.N. Lightfoot (2002). Transport Phenomena, *John Wiley & Sons*, New York, USA.

Brouwer, T., Lin, R.V., Kate, A.B., Schuur, B. and G. Bargeman (2021). Influence of solvent and acid properties on the relative volatility and separation selectivity for extractive distillation of close-boiling acids. *Ind. Eng. Chem. Res*., **60:** 7406-7416.

Cai, J., Yin, H. and F. Guo (2020). Transport analysis of material gap membrane distillation desalination processes. *Desalination*, **481:** 114361.

Elhenawy, Y., Elminshawy. A.S., Bassyouni, M., Alhathal Alanezi, A. and E. Drioli (2020). Experimental and theoretical investigation of a new air gap membrane distillation module with a corrugated feed channel. *Journal of Membrane Science*, **594:** 117461.

Gaur, D., Singh, K., Upadhyaya, S. and S.O. Meena (2022). Experimental study for benzene/water removal by air gap membrane distillation. *Asian Journal of Water, Environment and Pollution*, **19(5):** 43-51.

Kalla, S., Upadhyaya, S. and K. Singh (2019). Principles and advancements of air gap membrane distillation. *Reviews in Chemical Engineering*, **35(7):** 817-859.

Kalla, S., Upadhyaya, S., Singh, K. and R. Baghel (2019a.). Development of heat and mass transfer correlations and recovery calculation for HCl–water azeotropic separation using air gap membrane distillation. *Chemical Papers*, **73(10):** 2449-2460.

Kalla, S., Baghel, R., Upadhyaya, S. and K. Singh (2019b). Experimental and mathematical study of air gap membrane distillation for aqueous HCl azeotropic separation. *Journal of Chemical Technology and Biotechnology*, **94(1):** 63-78.

Khan, W. (1990). An extension of Danckwerts theoretical surface renewal model to mass transfer at contaminated turbulent interfaces. *Mathematical and Computer Modelling*, **14(C):** 750-754.

Leaper, S., Abdel-Karim, A., Gad-Allah, T.A. and P. Gorgojo (2019). Air-gap membrane distillation as a one-step process for textile wastewater treatment. *Chemical Engineering Journal*, **360:** 1330-1340.

Manju, S. and S. Netramani (2017). Renewable energy integrated desalination: A sustainable solution to overcome future fresh-water scarcity in India. *Renewable and Sustainable Energy Reviews*, **73:** 594-609.

Pangarkar, B.L., Deshmukh, S.K. and P.V. Thorat (2016). Energy efficiency analysis of multi-effect membrane distillation (MEMD) water treatment. *International Journal of Chem Tech Research*, **9(5):** 279-289.

Pedram, S., Mortaheb, H.R. and F. Arefi-Khonsa (2019). Optimization of benzene removal by air gap membrane distillation using response surface methodology. *Journal of Water Supply: Research and Technology – AQUA*, **68(4):** 231-242.

Phattaranawik, J., Jiraratananon, R. and A.G. Fane (2003). Effect of pore size distribution and air flux on mass transport in direct contact membrane distillation. *Journal of Membrane Science*, **215(1-2):** 75-85.

Pui, W.K., Yusoff, R. and M.K. Aroua (2019). A review on activated carbon adsorption for volatile organic compounds (VOCs). *Reviews in Chemical Engineering*, **35(5):** 649-668.

Stähelin, P.M., Valério, A., Guelli Ulson de Souza, S., Maria de Arruda, da Silva, A., Borges Valle, J.A., and A. Ulson de Souza (2018). Benzene and toluene removal from synthetic automotive gasoline by mono and bicomponent adsorption process. *Fuel*, **231:** 45-52.

Upadhyaya, S., Singh. K., Chaurasia, S., Dohare, R.K. and M. Agarwal (2016). Mathematical and CFD modeling of vacuum membrane distillation for desalination. *Desalination and Water Treatment*, **57(26):** 11956-11971.

van Vliet, Michelle T.H., Jones, E.R., Flörke, M., Franssen, W.H.P., Hanasaki, N. and Y. Wada (2021). Global water scarcity including surface water quality and expansions of clean water technologies. *Environmental Research Letters*, **16(2):** 024020.

Zare, S. and A. Kargari (2018). Membrane Properties in Membrane Distillation. *In:* Emerging Technologies for Sustainable Desalination Handbook. pp. 107-156.

Zhao, X., Zeng, X., Qin, Y., Li, X., Zhu, T. and X. Tang (2018). An experimental and theoretical study of the adsorption removal of toluene and chlorobenzene on coconut shell derived carbon. *Chemosphere*, **206:** 285-292.